

# APPLICATION DATA SHEET

SEE ATTACHED BIBLIOGRAPHIC INFORMATION

Matthew G. Fishler

Gabriel A. Mouchawar

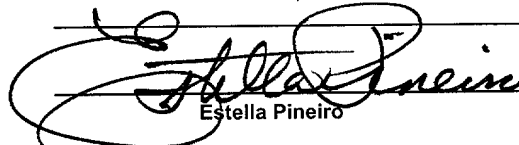
and

Mark W. Kroll

## SYSTEM AND METHOD OF GENERATING AN OPTIMAL THREE-STEP DEFIBRILLATION WAVEFORM FOR USE IN AN IMPLANTABLE CARDIOVERTER/DEFIBRILLATOR (ICD)

I hereby certify that this New Application is being deposited  
with the United States Postal Service as "Express Mail"  
mailing label number **EL758674946US**  
in an envelope as "Express Mail Post Office to Addressee"  
addressed to the:  
Assistant Commissioner for Patents  
Washington, D.C. 20231, on:

October 9, 2001

 10/9/01  
\_\_\_\_\_  
Estella Pineiro Date

Attorney Docket No. 98P1008US02

---

**SYSTEM AND METHOD OF GENERATING AN OPTIMAL  
THREE-STEP DEFIBRILLATION WAVEFORM FOR USE  
IN AN IMPLANTABLE CARIOVERTER/DEFIBRILLATOR (ICD)**

---

5

**Cross-Reference to Related Applications**

This application is a continuation-in-part (CIP) of U.S. Patent Application Serial No. 09/803,271, filed March 9, 2001, which claims the benefit of U.S. Patent Application Serial No. 09/073,394, filed May 5, 1998, which claims the benefit of U.S. Provisional Patent Application Serial No. 60/046,610, filed May 14, 1997.

10

**Field of the Invention**

The present invention relates to implantable medical devices, and more particularly to an implantable cardioverter defibrillator (ICD) configured to provide a high efficiency defibrillation waveform.

15

**Background of the Invention**

An ICD continues to be a relatively large device for implantation in the human body. The size of the ICD is primarily determined by the battery and capacitors used therein. The size of the battery (or batteries, in some instances) and capacitors, in turn, is determined by the shock energy requirements for a defibrillation pulse. Thus, a design approach that reduces the energy requirements for defibrillation results in a direct reduction in the overall ICD size.

20

In existing ICD devices, the defibrillation waveform or pulse used to deliver a defibrillation shock to the heart is generated by first charging the equivalent of a single capacitor (most ICDs use two capacitors connected in series to function as a single capacitor, thereby reducing the working voltage requirements for each capacitor of the series stack, as explained

25

below) to a desired charge level (voltage) and then discharging the single capacitor through the cardiac tissue for a prescribed period of time during a first or positive phase of the defibrillation waveform, and then reversing the polarity of the discharge for a second prescribed period of time during  
5 a second or negative phase of the defibrillation waveform, thereby producing a biphasic stimulation pulse or waveform. It should be noted that in this context the term "single capacitor" is used to refer to a single capacitance, which may be, and usually is obtained by a hardwired connection of two capacitors in series such that the two series capacitors  
10 always function and act as though they were a single capacitor. (Two or more capacitors are connected in series in this manner in order to achieve a higher working voltage for the series-connected capacitor. That is, when two capacitors are connected in series, and each has a working voltage of, e.g., 375 volts (V), then the overall or total working  
15 voltage of the series combination becomes 750 V.)

The purpose of applying a defibrillation shock to the heart is to shock the heart out of a state of fibrillation, or other non-functional state, into a functional state where it may operate efficiently as a pump to pump blood through the body. To this end, the positive phase of the biphasic  
20 waveform is preferably a very high voltage that serves to synchronously capture as many heart membrane cells as possible. See, Kroll, "A minimum model of the signal capacitor biphasic waveform" Pace, Nov. 1994. The negative phase of the biphasic waveform, in contrast, simply serves to remove the residual electrical charge from the membrane cells  
25 and bring the collective membrane voltage back to its original position or value. See, e.g., Kroll, *supra*; Walcott, et al., "Choosing The Optimal Monophasic and Biphasic Wave-Forms for Ventricular Defibrillation," Journal of Cardiovascular Electrophysiology (Sept. 1995). A biphasic pulse generator of the type used in an ICD device is shown, e.g., in U.S.  
30 Patent Nos. 4,850,357, issued to Bach, Jr.; and 5,083,562, issued to de Coriolis et al.

When a voltage shock is first applied to a membrane cell, the membrane does not respond to the shock immediately. Rather, the cell response lags behind the applied voltage. This time lag is more or less predictable in accordance with the Blair membrane model. See, e.g.,

5 Blair, "On the intensity-time relations for stimulation by electric currents. I" J. Gen Physiol., Vol. 15, pp. 709-729 (1932), and Blair, "On the intensity time relations for stimulation by electric currents. II", J. Gen Physiol., Vol. 15, pp. 731-755 (1932); Pearce et al., "Myocardial stimulation with ultrashort duration current pulses," PACE, Vol. 5, pp. 52-58 (1982).

10 When the applied voltage comprises a biphasic pulse having a constant voltage level for the duration of the positive phase (a condition achievable only when the voltage originates from an ideal battery), the membrane cell response to the positive phase reaches a peak (i.e., is at an optimum level) at the trailing edge of the positive phase. Unfortunately, when the

15 applied voltage originates from a charged capacitor, as is the case for an ICD device, the applied voltage waveform does not remain at a constant voltage level, but rather has a significant "tilt" or discharge slope associated therewith. Such tilt or slope causes the peak membrane cell response to occur at some point prior to the trailing edge of the positive

20 phase, which is less than optimum. What is needed, therefore, is a way to optimize the applied voltage waveform so that a maximum membrane cell response occurs coincident with, or nearly coincident with, the trailing edge of the positive phase.

It is known in the art to switch the capacitors of an ICD from a

25 parallel configuration during the positive phase of a biphasic defibrillation pulse to a series configuration during the negative phase of the biphasic defibrillation pulse. See, e.g., U.S. Patent Nos. 5,199,429 (FIG. 7A) and 5,411,525. While such action produces a defibrillation waveform having a somewhat different shape, i.e., a waveform having a leading edge voltage

30 of the second or negative phase which is approximately twice the trailing edge voltage of the first or positive phase, such action does little to

achieve a maximum cell membrane response coincident with the trailing edge of the first or positive phase.

It is also known in the art to sequentially switch capacitors in an ICD device in order to allow waveform "tailoring", e.g., prolong the positive phase duration by sequentially switching in a second charged capacitor as shown in **FIG. 9** of U.S. Patent No. 5,199,429, or by sequentially switching in second, third and fourth charged capacitors, as shown in FIG. 6C of U.S. Patent No. 5,199,429. However, such "tailoring" still does not address the main concern of achieving a maximum cell membrane response coincident with the trailing edge of the positive phase.

It is thus evident that what is needed is a capacitor switching scheme and/or method for use within an ICD device which achieves a maximum cell membrane response near or coincident with the trailing edge of the positive phase.

It is also desirable to provide an ICD that is as small as possible. The limiting factor on ICD thickness is the diameter of the high-energy capacitors. As indicated above, current ICDs typically use two electrolytic capacitors. Current technology in electrolytic capacitors limits the stored voltage to about 450 V per capacitor. Therefore, the current approach is to use two large (200  $\mu$ F or more) capacitors to achieve the stored energy of 25J - 40J required for defibrillation. Therefore, the thickness of the ICD is determined by the thickness of the large capacitors. There is thus a need for an ICD construction, which would permit the needed energy for defibrillation to be stored in the ICD, while allowing a thinner ICD thickness.

The inventions described in the aforementioned parent patent application (U.S. Patent Application No. 09/073,394) advantageously address the above and other needs. In particular, the parent patent application described a technique for generating a highly efficient biphasic defibrillation pulse by switching at least two charged capacitors from a

parallel connection to various combinations of a parallel/series connection or a series connection during the first phase of the defibrillation pulse. Such mid-stream parallel/series connection changes of the capacitors and steps up the voltage applied to the cardiac tissue during the first phase. A stepped-up voltage during the first phase, in turn, gives an extra boost to, and thereby forces additional charge (current) into, the cardiac tissue cells, and thereby transfers more charge to the membrane of the excitable cardiac cell than if the capacitors were continuously discharged in series. Phase reversal is timed with the cell membrane reaching its maximum value at the end of the first phase.

Although the technique of the parent application is quite effective, room for improvement remains. In particular, it would be desirable to provide a technique for generating a defibrillation waveform that requires even less shock energy to reach the myocardial defibrillation threshold so that battery power can be saved and device longevity improved, while still providing effective defibrillation. Moreover, it would be desirable to provide a technique for generating a defibrillation waveform, which reduces the total time, required to reach the myocardial defibrillation threshold thereby permitting the patient to be defibrillated more quickly. It is to these ends that aspects of the invention of the present CIP patent application are primarily directed.

### **Summary of Invention**

In accordance with a first aspect of the invention, increased myocardial voltage is achieved by a defibrillator configured to generate a defibrillation pulse waveform wherein a first (typically positive) phase of the waveform has at least three distinct voltage peaks. In one embodiment, the defibrillator includes a shocking circuit having a set of first, second and third capacitors and switching circuitry for selectively discharging the capacitors so as to generate the defibrillation pulse waveform having the three-peak positive phase. To this end, the

switching circuitry generates a first step of the pulse waveform by  
discharging the capacitors while all three capacitors are connected in  
parallel, then generates a second step of the pulse waveform by  
discharging the capacitors while the first and second capacitors are  
5 connected in parallel and the third capacitor is connected in series, and  
finally generates a third step of the pulse waveform by discharging the  
capacitors while all three capacitors are connected in series.

Preferably, the switching circuitry is configured to discharge the  
capacitors during the three steps of the pulse waveform for first, second  
10 and third time periods selected to maximize the final myocardial voltage  
within myocardial tissue receiving the pulse waveform. To maximize the  
final myocardial voltage, the first, second and third time periods are set to:

$$d_1^{opt} = -\frac{\tau_m}{\alpha_1} \cdot \ln \left\{ \left( \frac{\tau_m}{\tau_{s1}} \right) \left( \frac{2 - \frac{\alpha_2}{\alpha_1}}{1 - \frac{\alpha_2}{\alpha_1}} \right) \right\};$$

$$d_2^{opt} = +\frac{\tau_m}{\alpha_2} \cdot \ln \left\{ \left( \frac{1}{2} \right) \left( \frac{2 - \frac{\alpha_2}{\alpha_1}}{1 - \frac{\alpha_2}{\alpha_1}} \right) \left( \frac{1 - \frac{\alpha_3}{\alpha_2}}{K_C - \frac{\alpha_3}{\alpha_2}} \right) \right\}; \text{ and}$$

$$15 \quad d_3^{opt} = -\frac{\tau_m}{\alpha_3} \cdot \ln \left\{ \left( K_C \right) \left( \frac{1 - \frac{\alpha_3}{\alpha_2}}{K_C - \frac{\alpha_3}{\alpha_2}} \right) \right\}; \text{ wherein}$$

$$K_C = 1 + (C_C) / (C_A + C_B + C_C);$$

$$\alpha_1 = 1 - (\tau_m / \tau_{s1}), \alpha_2 = 1 - (\tau_m / \tau_{s2}), \text{ and } \alpha_3 = 1 - (\tau_m / \tau_{s3});$$

$$\tau_{s1} = R_s \cdot C_{s1}; \tau_{s2} = R_s \cdot C_{s2}; \text{ and } \tau_{s3} = R_s \cdot C_{s3};$$

$$C_{s1} = C_A + C_B + C_C;$$

$$20 \quad C_{s2} = [(C_A + C_B) \cdot (C_C)] / [C_A + C_B + C_C];$$

$$C_{s3} = 1 / \left[ \frac{1}{C_A} + \frac{1}{C_B} + \frac{1}{C_C} \right];$$

$C_A$ ,  $C_B$ , &  $C_C$  are the capacitances of the first, second and third capacitors, respectively; and  $\tau_m$  is a predetermined myocardial tissue time constant.

Also, preferably, the capacitances are selected so as to minimize the amount of energy required to be stored within the capacitors while still achieving the maximum final myocardial voltage. To minimize the amount of energy, the capacitances of the first, second and third time capacitors are set to:

$$C_A^{opt} = 0.6673 \cdot \left( \frac{\tau_m}{R_s} \right);$$

$$C_B^{opt} = 0.6673 \cdot \left( \frac{\tau_m}{R_s} \right); \text{ and}$$

$$C_C^{opt} = 1.5356 \cdot \left( \frac{\tau_m}{R_s} \right); \text{ wherein}$$

$R_s$  is a predetermined system resistance.

Using these capacitance values, the optimal first, second and third time periods  $d_1^{opt}$ ,  $d_2^{opt}$ , and  $d_3^{opt}$  for use in maximizing the myocardial potential may be simplified to:

$$d_1^{opt} = 0.878 \cdot \tau_m;$$

$$d_2^{opt} = 0.277 \cdot \tau_m; \text{ and}$$

$$d_3^{opt} = 0.200 \cdot \tau_m.$$

By employing a three capacitor shocking circuit configured as just summarized, the amount of energy required to reach a myocardial defibrillation threshold is less than for one-capacitor or two-capacitor systems, regardless of the total capacitance of the system. Hence, power can be saved, while still providing effective defibrillation. Moreover, the



total time required to reach the myocardial defibrillation threshold is less than with one-capacitor or two-capacitor systems, permitting the patient to be defibrillated more quickly. Additionally, the aforementioned three-capacitor system is generally less influenced by variations in underlying parameters and operating conditions and hence is generally more reliable.

In accordance with a second aspect of the invention, a method is provided for making and using an ICD capable of generating the improved defibrillation pulse waveform. In one embodiment, capacitances are selected for capacitors of a shocking circuit for use within the ICD. Optimal time periods for three steps of the positive phase of the defibrillation pulse to be generated by the shocking circuit are then determined, with the time durations being determined so as to maximize a final myocardial voltage within myocardial tissue receiving a pulse waveform from the shocking circuit based on initial capacitor voltages. An ICD is then fabricated having a shocking circuit employing capacitors having the selected capacitances and the shocking circuit is configured to be capable of selectively discharging the capacitors to generate a defibrillation pulse waveform having step durations equal to the optimal time periods. The ICD is implanted within a patient and is activated to detect defibrillation. The shocking circuit is controlled to generate the defibrillation pulse having the three-step positive phase upon detection of fibrillation. In this manner, maximum myocardial voltage can be achieved within myocardial tissue connected to the ICD.

#### **Brief Description of the Drawings**

The above and other aspects, features, and advantages of the present invention will be more apparent from the following more particular description thereof, presented in conjunction with the following drawings, wherein:

**FIG. 1** illustrates a preferred defibrillation biphasic pulse or waveform generated in accordance with a two-capacitor ICD in accordance with the present invention;

**FIG. 2** depicts the excitable cardiac membrane response to the waveform of **FIG. 1**;

**FIG. 3** is a functional block diagram of a two-capacitor ICD device, which generates the waveform of **FIG. 1**;

**FIG. 4** is a simplified schematic diagram of a three-capacitor ICD made in accordance with the invention;

**FIG. 5** illustrates one type of defibrillation waveform that may be generated using the ICD of **FIG. 4**;

**FIG. 6** depicts the excitable cardiac membrane response during phase 1 (positive phase) to the waveform of **FIG. 5**;

**FIG. 7** illustrates another type of defibrillation waveform that may be generated using the ICD of **FIG. 4**;

**FIG. 8** depicts the excitable cardiac membrane response during phase 1 (positive phase) to the waveform of **FIG. 7**;

**FIG. 9** illustrates, for comparative purposes, the biphasic defibrillation waveform typically provided by a two-capacitor ICD of the prior art;

**FIG. 10** illustrates, again for comparative purposes, the membrane response during phase 1 (positive phase) to the waveform of **FIG. 9**.

**FIG. 11** shows the first phase of a parallel/series discharge waveform with the durations and time constants defined;

**FIG. 12** shows a first contour plot of stored energy as a function of a scaling factor "K" (equivalent to  $C_A/C_B$  and the total capacitance ( $C_A/C_B$  as scaled by  $\tau_m/R_S$ );

**FIGS. 13 and 14** show a second and third contour plot of the  $d_1$  and  $d_2$ , respectively, as a function of the scaling factor  $K$  and the total capacitance, wherein the optimal value occurs at the cross-hair;

**FIGS. 15, 16 and 17** illustrate how the optimal values for  $d_1$  and  $d_2$ ,  
5 tissue resistance ( $R_S$ ) and tissue time constants ( $\tau_m$ );

**FIG. 18** is a graph of optimal durations for  $d_1$  and  $d_2$  as a function of tissue resistance ( $R_S$ ) for desired (e.g., 60  $\mu$ F) capacitor and a range of tissue time constants ( $\tau_m$ );

**FIG. 19** illustrates a single-step and a two-step (parallel/series)  
10 waveform of equal stored energy and their resulting cell membrane responses;

**FIG. 20** illustrates the single-step and the two-step waveforms normalized to achieve the maximum cell member response;

**FIGS. 21 and 22** illustrate analogous results to those depicted in  
15 **FIG. 20** albeit for extreme combinations of  $R_S$  and  $C_A (=C_B)$ ;

**FIG. 23** illustrates the general shape of a three-step defibrillation waveform that may be generated using the three-capacitor ICD of **FIG. 4**;

**FIG. 24** illustrates a specific exemplary defibrillation waveform having a three-step positive generated using the three-capacitor ICD of  
20 **FIG. 4**;

**FIG. 25** depicts the excitable cardiac membrane response during the defibrillation waveform of **FIG. 24**;

**FIG. 26** is a flow chart providing an overview of a technique for making an using an ICD for generating shocking pulses exploiting the  
25 defibrillation waveform of **FIG. 23**.

**FIG. 27** is a graph the ratio of individual capacitances to total capacitance as a function of the ratio of total capacitance to optimal

capacitance for the three-capacitor system used to generate the defibrillation waveform of **FIG. 23**;

**FIG. 28** is a graph the relative energy needed to reach a myocardial defibrillation threshold as a function of total capacitance for one-, two- and three-capacitor shocking circuits showing that the relative energy required is less for the three-capacitor shocking circuit for all values of total capacitance;

**FIG. 29** is a graph the total duration needed to reach the myocardial defibrillation threshold as a function of total capacitance for one-, two- and three-capacitor shocking circuits showing that the total time required is less for the three-capacitor shocking circuit for all values of total capacitance;

**FIG. 30** is a simplified diagram illustrating an implantable stimulation device in electrical communication with at least three leads implanted into a patient's heart for delivering shock therapy in accordance with any of the shocking pulse waveforms described herein; and

**FIG. 31** is a functional block diagram of the multi-chamber implantable stimulation device of **FIG. 30** illustrating the basic elements of a stimulation device which can provide cardioversion, defibrillation and pacing stimulation in four chambers of the heart.

### **Detailed Description of the Invention**

The following description is of the best mode currently contemplated for practicing the invention.

The basic concept of the invention relating to forming an efficient defibrillation waveform can be practiced with two or more capacitors within the ICD. A preferred number of capacitors is three. However, the basic concept will first be explained in the context of a two-capacitor ICD.

Pulse Generation Using Parallel/Series Capacitors

In accordance with one aspect of the invention, then a biphasic pulse or waveform is generated by an ICD device having two capacitors that includes a positive phase of duration  $t_1$  ms and a negative phase of duration  $t_2$  ms, as shown in **FIG. 1**. First and second capacitors,  $C_A$  and  $C_B$ , within the ICD device are initially charged to a voltage  $V_1$  and are connected in parallel. The biphasic defibrillation pulse begins by discharging the charged parallel capacitors through the cardiac tissue by way of defibrillation electrodes in contact with the cardiac tissue. Thus, a leading edge of the biphasic pulse starts at a first peak voltage of approximately  $V_1$  volts (the charge on the first and second capacitors when first connected to the electrodes).

During a first step or portion of the positive phase of the biphasic pulse, the amplitude of the biphasic pulse decays from the first peak voltage  $V_1$  to a voltage  $V_2$  in accordance with a first time constant  $\tau_1$ . The first time constant  $\tau_1$  varies as a function of  $(C_A + C_B)R$ , where  $C_A$  is the value of the first capacitor,  $C_B$  is the value of the second capacitor, and  $R$  is an effective resistance associated with the discharge through the first and second electrodes.

A second step or portion of the positive phase begins by connecting the first and second capacitors in series. This sudden series connection increases the defibrillation pulse to a second peak voltage of approximately  $2(V_2)$  volts (the sum of the voltages on each of the first and second capacitors at the time the series connection is made), as illustrated in **FIG. 1**. The amplitude of the biphasic pulse decays during the second portion of the positive phase from the second peak voltage  $2(V_2)$  to a voltage  $V_3$  in accordance with a second time constant  $\tau_2$ . The second time constant  $\tau_2$  varies as a function of  $(C_A C_B / C_A C_B)R$ . Advantageously, the voltage at the trailing edge of the positive phase,  $V_3$ , occurs at a time that is near the maximum cell membrane response.

The negative phase of the biphasic waveform begins by inverting the polarity of the series-connected first and second capacitors. Such negative phase thus commences at a third peak voltage of approximately -V<sub>3</sub> volts, and decays thereafter towards zero in accordance with the second time constant  $\tau_2$ . After a prescribed time period  $t_2$ , the negative phase ends.

The biphasic waveform produced in accordance with the two-capacitor ICD is illustrated in **FIG. 1**. The first portion of the positive phase may terminate when either: (1) the voltage decreases below a threshold voltage V<sub>3</sub>; or (2) a prescribed time period  $t_a$  has elapsed.

The tissue membrane voltage that results when the waveform of **FIG. 1** is applied to excitable cardiac tissue membranes is as shown in **FIG. 2**. This membrane voltage is obtained by modeling the tissue membranes as taught in the Blair reference, previously cited. As shown in **FIGS. 11-20**, the optimum duration for  $t_a$  will be described in more detail.

A functional block diagram of the pulse generation circuitry used to generate the biphasic waveform of the two-capacitor ICD is shown in **FIG. 3**.

As seen in **FIG. 3**, a cardiac tissue-stimulating device 10 includes a power source 12, e.g., at least one battery, a timing and control circuit 14, a charging circuit 16, an isolation switch network SW1, a series parallel switch network SW2, at least two capacitors C<sub>A</sub> and C<sub>B</sub>, an output switch network SW3, and at least two electrodes 20 and 22. The electrodes 20 and 22 are adapted to be positioned within or on the heart. The electrodes 20 and 22 are connected to the output switch SW3 through conventional leads 21 and 23, respectively.

A voltage sense amplifier 24 senses the voltage held on the capacitor C<sub>B</sub> (which will be the same voltage as capacitor C<sub>A</sub> when C<sub>A</sub> and C<sub>B</sub> are connected in parallel). In some embodiments of the invention,

a current sense amplifier 26 may also be used to sense the current flowing to or returning from one of the electrodes 20 or 22. In **FIG. 3**, such current is sensed by differentially measuring the voltage across a small current-sense resistor  $R_S$  connected in series with electrode 22.

- 5 The outputs of the voltage sense amplifier 24 and the current sense amplifier 26 are directed to the timing and control circuit 14.

A suitable cardiac activity sensor 28 is also employed within the device 10 in order to detect cardiac activity. The function of the sensor 28 is to sense cardiac activity so that an assessment can be made by the  
10 timing and control circuitry whether a defibrillation pulse needs to be generated and delivered to the cardiac tissue. Such sensor 28 may take many forms, e.g., a simple R-wave sense amplifier of the type commonly employed in implantable pacemakers. The details of the sensor 28 are not important for purposes of the present invention.

- 15 The power source 12 is connected to provide operating power to all components and circuitry within the device 10. The power source 12 also provides the energy needed to generate the biphasic defibrillation pulse. That is, energy stored within the power source 12 is used to charge capacitors  $C_A$  and  $C_B$ , through the charging circuit 18, up to the  
20 desired initial defibrillation starting pulse voltage  $V_1$ . Such charging is carried out under control of the timing and control circuit 14. Typically,  $V_1$  may be a relatively high voltage, e.g., 375 volts, even though the power source 12 may only be able to provide a relatively low voltage, e.g., 3-6 volts. The charging circuit 16 takes the relatively low voltage from the  
25 power source 12 and steps it up to the desired high voltage  $V_1$ , using conventional voltage step-up techniques as are known in the art. This stepped-up voltage  $V_1$  is then applied through the isolation switch SW1 to both capacitors  $C_A$  and  $C_B$  at a time when  $C_A$  and  $C_B$  are connected in parallel, i.e., when SW2 is in its P position, and at a time when the output  
30 switch is in its open, or OFF, position. As the capacitors  $C_A$  and  $C_B$  are being charged, the voltage sense amplifier 24 monitors the voltage level

on the capacitors. When the desired voltage  $V_1$  has been reached, the timing and control circuitry 14 turns off the charging circuit 16 and opens the isolation switch SW1, thereby holding the voltage  $V_1$  on capacitors  $C_A$  and  $C_B$  until such time as a defibrillation pulse is needed.

5           When a defibrillation pulse is called for by the timing and control circuit 14, the output switch SW3 is placed in its positive phase position, POS, thereby connecting the parallel connected capacitors  $C_A$  and  $C_B$  (on which the starting voltage  $V_1$  resides) to the cardiac tissue through the electrodes 20 and 22. Such connection starts the discharge of  
10           capacitors  $C_A$  and  $C_B$  through the cardiac tissue in accordance with the first time constant  $\tau_1$  as described above in connection in **FIG. 1**.

          After a period of time  $t_a$ , or as soon as the voltage across the parallel-connected capacitors  $C_A$  and  $C_B$  has decreased to the threshold value  $V_2$  (as sensed by the voltage sense amplifier 24), the timing and  
15           control circuit switches SW2 to its series-connected or S position, thereby connecting the capacitors  $C_A$  and  $C_B$  in series across the electrodes 20 and 22. Such series connection doubles the voltage across the electrodes 20 and 22 to a value of  $2(V_2)$ . Thereafter, the discharge of the series-connected capacitors  $C_A$  and  $C_B$  continues through the cardiac  
20           tissue in accordance with the second time constant  $\tau_2$  as described above. This discharge continues until the end of the positive phase.

          The positive or first phase ends at a time  $t_1$  from the beginning of the positive phase (as measured by timing circuits within the timing and control circuit 14), or when the voltage has decayed to a value  $V_3$  (as  
25           sensed by voltage sense amplifier 24). Alternatively, the positive phase may end as a function of the sensed current (as sensed by the current sense amplifier 26), e.g., at a time when the sensed current has decreased from a peak value by a prescribed amount or percentage.

          As soon as the positive phase ends, the timing and control circuit  
30           14 switches the output switch SW3 to the negative phase position, NEG,



thereby reversing the polarity of the discharge of the series-connected capacitors  $C_A$  and  $C_B$  through the cardiac tissue. The negative phase lasts thereafter for a time period  $t_2$  determined by the timing and control circuitry.

5           The functions represented by the functional block diagram of **FIG. 3** may be implemented by those of skill in the art using a wide variety of circuit elements and components. It is not intended that the present invention be directed to a specific circuit, device or method; but rather that  
10           any circuit, device or method which implements the functions described above in connection with **FIG. 3** to produce a defibrillation waveform of the general type shown in **FIG. 1** be covered by the invention.

Turning next to **FIG. 4**, there is shown a simplified schematic diagram of an ICD having three 120  $\mu$ F capacitors  $C_1$ ,  $C_2$  and  $C_3$ . The manner of charging the capacitors while they are connected in parallel is  
15           the same or similar to that shown in **FIG. 3**. When the capacitors  $C_1$ ,  $C_2$  and  $C_3$  have been charged to a high voltage, e.g., 370 V, a stored energy of approximately 25 joules is realized. Once the capacitors have been charged by the ICD, the capacitors are configured for a parallel  
20           discharge. This is accomplished by closing switches  $S_1$ ,  $S_2$ ,  $S_3$  and  $S_4$ , while maintaining switches  $S_5$  and  $S_6$  open. The parallel discharge takes place from time  $t=0$  until a time  $d_1$ . Once  $d_1$  elapses, one of two options may be used to discharge the remaining charge.

In accordance with a first option, or Option 1, after  $d_1$  has elapsed (i.e., after the capacitors are discharged in parallel until time  $d_1$ ), all of the  
25           capacitors are discharged in series for the remainder of the pulse. This is accomplished by opening  $S_1$ ,  $S_2$ ,  $S_3$  and  $S_4$  and closing  $S_5$  and  $S_6$ . At a later time,  $d_2$ , the "H Bridge" circuit 40 (**FIG. 4**) is used to reverse the polarity of the output. At yet a later time,  $d$ , the output pulse is truncated.

The waveform generated in accordance with Option 1 is illustrated  
30           in **FIG. 5**. The tissue membrane voltage associated with the waveform of

**FIG. 5** is modeled and computed, using the Blair model, as shown in **FIG. 6**. For the example shown in **FIGS. 5** and **6**, the optimum value of  $d_1$  is nominally about 3.5 ms. The optimum choice of  $d_2$  is when the elapsed time at  $d_2$  is about 1.5 times the elapsed time at  $d_1$ , or when the elapsed time at  $d_2$  (from  $t=0$ ) is about 5.25 ms.

In accordance with a second option, or Option 2, the capacitors C1 and C2 remain in parallel and are in series with C3 until time  $d_2$ . This is accomplished by opening S3 and S4 and closing S6. After  $d_2$  all the capacitors are in series (S1 and S2 also open, S5 closed) until C3 runs out of charge at a time  $d_4$ . After  $d_4$ , the diode D<sub>1</sub> bypasses the depleted capacitor and the time constant of discharge is of C1 and C2 in series. At a time  $d_3$ , where  $d_2 < d_3 < d_4$ , the polarity of the output is reversed using the H Bridge 40. The pulse is truncated at time  $d$ . The resulting waveform is shown in **FIG. 7**. The resulting membrane voltage is modeled and computed and shown in **FIG. 8**.

For the example shown in **FIGS. 7** and **8**, the optimum values of  $d_1$  is 2.7 ms,  $d_2$  is 1.5 times  $d_1$  (or about 4 ms),  $d_3$  is  $d_2 + 1.25$  ms. The value of  $d_4$  is computed to be about 7.6 ms. The choice of  $d$  can be in the range of 1.5 to 2.0 times that of  $d_3$ .

With either Option 1 or Option 2, the choice of the values  $d_1$ ,  $d_2$  and  $d_3$  are primarily functions of the ICDs capacitance value, the discharge pathway impedance, and the tissue time constant ( $\tau_m$ ).

The advantage of Option 2 is that the peak waveform voltage is lower than Option 1 yet a minute increase in membrane voltage over Option 1 is achieved. However, Option 1 is simpler to implement and diode D<sub>1</sub> is not needed since all the capacitors are discharged equally.

The advantages of either Option 1 or Option 2 are better appreciated by comparing the results of such discharge, as presented in **FIGS. 5, 6, 7** and **8**, with the corresponding discharge achieved with a two-capacitor ICD series discharge, as is commonly used in a

conventional ICD of the prior art. The discharge waveform achieved with a conventional two-capacitor ICD using series discharge, and the resulting membrane voltage, is shown in **FIGS. 9** and **10**, respectively.

Note, that to store equal energy to the three capacitor ICD, each

5 capacitor of the two-capacitor ICD must have 1.5 times the capacitance value, or two capacitors each with  $C=180\ \mu\text{F}$ .

As can be seen from a comparison of **FIGS. 9** and **10** with **FIGS. 5** and **6** (Option 1), and 5A and 5B (Option 2), for equal stored energy, the value of the peak membrane voltage for Option 2 is 1.18 times higher  
10 than the membrane voltage realized using the conventional waveform. Similarly, Option 1 yields a membrane voltage that is 1.17 times higher than is realized using the conventional waveform. In other words, a 25 joule ICD with three  $120\mu\text{F}$  capacitors and a switching network as in Option 2 performs equally to a 34.4 joule conventional ICD with two  
15  $180\mu\text{F}$  capacitors. This represents a remarkable improvement in performance.

As shown in **FIG. 11**, the two-step waveform has been reproduced.

Although identical in nature to that shown in **FIG. 1**, the designators have been changed slightly for purposes of the in depth analysis that will  
20 follow.

As described above in conjunction with **FIG. 3**, two capacitors,  $C_A$  &  $C_B$ , have been charged to the same initial voltage,  $V_{01}$ . The system resistance (as seen by device) is given by  $R_s$ . For purposes of this discussion, the myocardium has been modeled as a parallel-RC circuit  
25 with myocardial tissue time constant,  $\tau_m$ .

The amplitude of each step of the positive portion of the defibrillation waveform, shown in **FIG. 11**, can be characterized with the following basic equations:

$$\begin{aligned} V_{s1}(t_1) &= V_{01} \cdot \exp[-t_1/\tau_{s1}] & 0 \leq t_1 \leq d_1 \\ V_{s2}(t_2) &= V_{02} \cdot \exp[-t_2/\tau_{s2}] & 0 \leq t_2 \leq d_2 \end{aligned}$$

5 wherein:

$V_{s1}$  is the exponential decay during the first period,  $t_1$ , (i.e., Step1);

$V_{s2}$  is the exponential decay during the second period,  $t_2$ , (i.e., Step2);

$\tau_{s1}$  is the time constant of  $C_A$  and  $C_B$  in parallel;

$\tau_{s2}$  is the time constant of  $C_A$  and  $C_B$  in series;

10  $V_{01}$  is the initial voltage during Step1 on the capacitors  $C_A$  and  $C_B$  once fully charged to the source voltage,  $V_{01}$ ; and

$V_{02}$  is the initial voltage during Step2 remaining on the capacitors  $C_A$  and  $C_B$ , now configured in series.

15 The analysis that follows directly will explain how to determine the absolute and approximate solutions for the optimal durations,  $d_1$  and  $d_2$ , to maximize induced myocardial potential,  $V_m(t)$ , when the two capacitors are arranged in a parallel-series, two-step arrangement.

20 Consider the myocardial responses to  $V_{s1}(t_1)$  [Step1] and  $V_{s2}(t_2)$  [Step2] separately. Note that the following derivations (Equations 1-4) make absolutely *no* assumptions regarding any specific relationships between the characteristics of Step1 and Step2.

The "Step1" myocardial response,  $V_{m1}$ , to the Step1 waveform,  $V_{s1}$ , is described by:

$$25 \quad \frac{dV_{m1}(t_1)}{dt_1} + \frac{V_{m1}(t_1)}{\tau_m} \propto \frac{V_{s1}(t_1)}{\tau_m} \quad (\text{Eq. 1})$$

with the initial condition:  $V_{m1}(0) = 0$ .

The solution to this differential equation is:

$$V_{m1}(t_1) = \begin{cases} \frac{V_{01}}{\alpha_1} \cdot \left( \exp\left[\frac{-t_1}{\tau_{s1}}\right] - \exp\left[\frac{-t_1}{\tau_m}\right] \right) & \tau_{s1} \neq \tau_m \\ \frac{V_{01}}{\tau_{s1}} \cdot \left( t_1 \cdot \exp\left[\frac{-t_1}{\tau_{s1}}\right] \right) & \tau_{s1} = \tau_m \end{cases} \quad (\text{Eq. 2})$$

where  $\alpha_1 = 1 - (\tau_m / \tau_{s1})$ .

The "Step2" myocardial response,  $V_{m2}$ , to the Step2 waveform,  $V_{s2}$ , is governed by:

$$5 \quad \frac{dV_{m2}(d_1, t_2)}{dt_2} + \frac{V_{m2}(d_1, t_2)}{\tau_m} \propto \frac{V_{s2}(t_2)}{\tau_m} \quad (\text{Eq. 3})$$

with the initial condition:  $V_{m2}(d_1, 0) = V_{m1}(d_1)$ , where  $d_1$  represents the final duration of Step1.

10 This initial condition ensures that there is a continuity of myocardial voltage when transitioning from the end of Step1 into the start of Step2.

The solution to this differential equation is:

$$V_{m2}(d_1, t_2) = V_{m1}(d_1) \cdot \exp\left[\frac{-t_2}{\tau_m}\right] + \begin{cases} \frac{V_{02}(d_1)}{\alpha_2} \cdot \left( \exp\left[\frac{-t_2}{\tau_{s2}}\right] - \exp\left[\frac{-t_2}{\tau_m}\right] \right) & \tau_{s2} \neq \tau_m \\ \frac{V_{02}(d_1)}{\tau_{s2}} \cdot \left( t_2 \cdot \exp\left[\frac{-t_2}{\tau_{s2}}\right] \right) & \tau_{s2} = \tau_m \end{cases} \quad (\text{Eq. 4})$$

15 where  $\alpha_2 = 1 - (\tau_m / \tau_{s2})$ , and  $V_{02}$  is proportional to  $V_{s2}(0)$ .

Equation (4) describes a curve with a single maximum value. The step durations,  $d_1 = d_1^{opt}$  and  $d_2 = d_2^{opt}$ , that maximize this shock-induced myocardial voltage,  $V_{m2}(t_1, t_2)$ , can be determined by solving the simultaneous equations given by:

20

$$\frac{\partial V_{m2}(d_1^{opt}, d_2^{opt})}{\partial d_1^{opt}} = 0 \quad \frac{\partial V_{m2}(d_1^{opt}, d_2^{opt})}{\partial d_2^{opt}} = 0 \quad (\text{Eq. 5})$$

From Equation (5), two equations that describe  $d_2^{opt}$  as a function of  $d_1^{opt}$  can be found (the following derivations assume  $\tau_{s1} \neq \tau_m$  and  $\tau_{s2} \neq$

5  $\tau_m$ ):

$$d_2^{opt} = \frac{\tau_m}{\alpha_2} \cdot \ln \left\{ 1 + \left( \frac{\alpha_2}{\alpha_1} \cdot \frac{V_{01}}{\partial V_{02} / \partial d_1^{opt}} \right) \cdot \left( \frac{1}{\tau_{s1}} \exp \left[ \frac{-d_1^{opt}}{\tau_{s1}} \right] - \frac{1}{\tau_m} \exp \left[ \frac{-d_1^{opt}}{\tau_m} \right] \right) \right\} \quad (\text{Eq. 6})$$

$$d_2^{opt} = \frac{\tau_m}{\alpha_2} \cdot \ln \left\{ \frac{\tau_{s2}}{\tau_m} \left[ 1 - \left( \frac{\alpha_2}{\alpha_1} \cdot \frac{V_{01}}{V_{02}(d_1^{opt})} \right) \cdot \left( \exp \left[ \frac{-d_1^{opt}}{\tau_{s1}} \right] - \exp \left[ \frac{-d_1^{opt}}{\tau_m} \right] \right) \right] \right\} \quad (\text{Eq. 7})$$

10 Setting Equations (6) and (7) equal to each other and simplifying produces the following implicit equation for  $d_1^{opt}$ :

$$\left( \frac{\tau_m}{\tau_{s2}} \cdot \frac{\alpha_1}{V_{01}} \right) = \left( \frac{1/\tau_{s1}}{\partial V_{02} / \partial d_1^{opt}} + \frac{\tau_{s2}/\tau_m}{V_{02}(d_1^{opt})} \right) \exp \left[ \frac{-d_1^{opt}}{\tau_{s1}} \right] - \left( \frac{1/\tau_m}{\partial V_{02} / \partial d_1^{opt}} + \frac{\tau_{s2}/\tau_m}{V_{02}(d_1^{opt})} \right) \exp \left[ \frac{-d_1^{opt}}{\tau_m} \right] \quad (\text{Eq. 8})$$

15 Further simplifications of Equation (8) require that  $V_{02}(d_1)$  be explicitly defined.

When the two system capacitors ( $C_A$  &  $C_B$ ) are configured into a parallel arrangement during Step1 and then reconfigured into a series arrangement during Step2, the system time constants can be explicitly defined as:

$$20 \quad \tau_{s1} = R_s \cdot (C_A + C_B) \quad \tau_{s2} = R_s \cdot (C_A C_B) / (C_A + C_B) \quad (\text{Eq. 9})$$

Furthermore,  $V_{02}(d_1)$  is explicitly defined as:

$$\begin{aligned} V_{02}(d_1) &= 2 \cdot V_{s1}(d_1) \\ &= 2 \cdot V_{01} \cdot \exp[-d_1/\tau_{s1}] \end{aligned} \quad (\text{Eq. 10})$$

where Equation (10) codifies the notion that, in a parallel-series  
5 arrangement, the leading edge voltage of Step2 equals twice  
the trailing edge voltage of Step1.

Substituting Equation (10) into Equation (8) and solving explicitly  
for  $d_1^{opt}$  and subsequently  $d_2^{opt}$  [via Equation (6) or (7)] yields:

$$d_1^{opt} = -\frac{\tau_m}{\alpha_1} \cdot \ln \left\{ \left( \frac{\tau_m}{\tau_{s1}} \right) \left( \frac{2\alpha_1 - \alpha_2}{\alpha_1 - \alpha_2} \right) \right\} \quad (\text{Eq. 11})$$

$$d_2^{opt} = +\frac{\tau_m}{\alpha_2} \cdot \ln \left\{ \left( \frac{1}{2} \right) \left( \frac{2\alpha_1 - \alpha_2}{\alpha_1 - \alpha_2} \right) \right\} \quad (\text{Eq. 12})$$

The maximum myocardial voltage attained using these optimal  
parallel-series step durations can then be determined by substituting  
15 Equations (10)-(12) into Equation (4) and simplifying:

$$V_{m2}(d_1^{opt}, d_2^{opt}) = V_{01} \left( \frac{1}{2} \right)^{\frac{1}{\alpha_2}} \left( \frac{\tau_m}{\tau_{s1}} \right)^{\frac{1}{\alpha_1} - 1} \left( \frac{2\alpha_1 - \alpha_2}{\alpha_1 - \alpha_2} \right)^{\frac{1}{\alpha_1} - \frac{1}{\alpha_2}} \quad (\text{Eq. 13})$$

Note that Equations (11)-(13) are valid for *any independent values* of  $C_A$   
and  $C_B$ .

20 According to this simple RC model of defibrillation, successful  
defibrillation is achieved when the myocardial voltage (as embodied  
herein by  $V_{m1}$  and  $V_{m2}$ ) is "depolarized" to its threshold value,  $V_{th}$ . An  
equation that describes the minimum relative magnitude for  $V_0$  (i.e., the  
voltage to which each of the capacitors is charged in preparation for the  
25 defibrillation shock) that successfully drives  $V_{m2}$  to  $V_{th}$  can be obtained

from Equation (13) by setting  $V_{m2} = V_{th}$  and solving for  $V_{01}$  (which, for these parallel-series shocks, is equivalent to  $V_0$ ).

Since the total stored energy in capacitors  $C_A$  and  $C_B$  is given by:

$$E_{stored} = \frac{1}{2}(C_A + C_B) \cdot V_0^2 \quad (\text{Eq. 14})$$

5

then the optimal relationship between  $C_A$  and  $C_B$  that maximizes myocardial voltage for a given total stored energy can be found by substituting  $C_A = k \cdot C_B$  into Equation (14) and then solving for  $k$  in  $\partial E_{stored} / \partial k = 0$ . The result is:

$$10 \quad k^{opt} = C_A / C_B = 1 \quad (\text{Eq. 15})$$

The above result implies that  $C_A$  should equal  $C_B$  in order to achieve maximum myocardial impact for any given total energy. The relationship  $C_A = C_B$  is equivalent to  $\tau_{s1} = 4 \cdot \tau_{s2}$  [see Equation (9)], from which simplified

15 versions of Equations (11)-(13) can be derived:

$$d_1^{opt} = -\frac{\tau_m}{\alpha_1} \cdot \ln \left\{ \left( \frac{1}{3} \right) \left( 1 + \frac{\tau_m}{2\tau_{s2}} \right) \right\} \quad (\text{Eq. 16})$$

$$d_2^{opt} = +\frac{\tau_m}{\alpha_2} \cdot \ln \left\{ \left( \frac{1}{3} \right) \left( 1 + \frac{2\tau_{s2}}{\tau_m} \right) \right\} \quad (\text{Eq. 17})$$

$$V_{m2}(d_1^{opt}, d_2^{opt}) = 2V_{01} \left( \frac{\tau_m}{2\tau_{s2}} \right)^{\frac{1}{\alpha_2}-1} \left[ \left( \frac{1}{3} \right) \left( 1 + \frac{\tau_m}{2\tau_{s2}} \right) \right]^{\frac{1}{\alpha_1}-\frac{1}{\alpha_2}} \quad (\text{Eq. 18})$$

20 Finally, the optimal capacitance for a given  $R_s$  and  $\tau_m$  is determined by finding the value of  $C_A$  that minimizes  $E_{stored}$ , that is, solving for  $C_A$  in  $\partial E_{stored} / \partial C_A = 0$  (with  $k = 1$ ). The result is:

$$C_A = C_B = \frac{\tau_m}{R_s} \quad (\text{Eq. 19})$$

or equivalently, the optimal capacitance (for a given  $R_s$  and  $\tau_m$ ) is that

25 which satisfies:

$$\frac{1}{2} \tau_{s1} = 2\tau_{s2} = \tau_m \quad (\text{Eq. 20})$$



Under these ideal conditions, the optimal step durations are:

$$d_1^{opt} = +2\tau_m \cdot \ln[3/2] \approx 0.811 \cdot \tau_m \quad (\text{Eq. 21})$$

$$d_2^{opt} = +\tau_m \cdot \ln[3/2] \approx 0.405 \cdot \tau_m \quad (\text{Eq. 22})$$

5

Further insights into the preceding theoretical calculations can be gleaned from corresponding graphical analyses. The relative stored energy required for defibrillation ( $E_{stored}$ ) for all possible parallel-series two-step waveforms is graphically illustrated in the contour plot of **FIG. 12**. In this plot, the x-axis is indexed by the total capacitance ( $C_A + C_B$ , scaled by  $\tau_m/R_s$ ) while the y-axis is indexed by the ratio of the two capacitances ( $k = C_A/C_B$ ). Although perhaps seemingly non-intuitive axis definitions, they efficiently provide complete coverage of the entire parameter space of all possible capacitor combinations for two-step waveforms. As indicated by the horizontal line 100 and the vertical line 102 overlaid on this plot (and as consistent with the conclusions of Equations (15) and (19)), the most efficient two-step positive portion for the biphasic shock is delivered when:

10

15

$$k = 1.0; \text{ and}$$

$$C_A + C_B = 2 \cdot \tau_m / R_s ;$$

which occurs at point 104 in **FIG. 12**.

The contours then step out from this optimal point in 1% increments, thus providing an indication as to the relative sensitivity of the energy efficiency to deviations in either total capacitance or capacitance ratio. In fact, energy efficiency remains quite robust: for example, energy efficiency remains within 1% of optimal for:

20

$$\sim 1.5 \cdot \tau_m / R_s < (C_A + C_B) < \sim 2.7 \cdot \tau_m / R_s ; \text{ and}$$

$$\sim 0.7 < k < \sim 1.4.$$

Two-dimensional contour plots of optimal Step1 and Step2 durations (normalized by  $\tau_m$ , i.e.,  $d_1^{opt}/\tau_m$  and  $d_2^{opt}/\tau_m$ ) as given by Equations (11) and (12) are presented in **FIGS. 13 and 14**, respectively.

Similar to **FIG. 12**, **FIGS. 13 and 14** have respective horizontal lines 110, 120 and vertical lines 112, 122 from have been overlaid on these contour maps as well. Their respective intersections 114, 124 appropriately correspond to the "0.811" and "0.405" coefficients found in Equations (21) and (22), respectively.

Since  $R_s$  and  $\tau_m$  represent patient-specific variables that directly impact the choice of durations used for these stepped waveforms, it is perhaps useful to present example values for  $d_1^{opt}$  and  $d_2^{opt}$  for a representative range of values for  $R_s$  (30-90  $\Omega$ ),  $\tau_m$  (2-4 ms), and  $C_A$  (30-90  $\mu F$ ). The tables shown in **FIGS. 15-17** provide such a set of example values, wherein values for  $d_1^{opt}$  and  $d_2^{opt}$  are computed from Equations (16) and (17), respectively.

Given the limits of the ranges used for  $R_s$ ,  $\tau_m$ , and  $C_A$  in the tables shown in **FIGS. 15-17**,  $d_1^{opt}$  and  $d_2^{opt}$  range from lows of 1.286 and 0.422 ms (when  $\tau_m = 2$  ms,  $C_A = 30$   $\mu F$ , and  $R_s = 30$   $\Omega$ ) to highs of 3.704 and 2.689 ms (when  $\tau_m = 4$  ms,  $C_A = 90$   $\mu F$ , and  $R_s = 90$   $\Omega$ ), respectively.

To summarize the above, for the ranges of:

$$\begin{aligned}\tau_m &= 2 - 4 \text{ ms;} \\ R_s &= 30 - 90 \Omega; \\ C_A &= C_B = 30 - 90 \mu F\end{aligned}$$

Then, the optimum durations fall in the ranges:

$$\begin{aligned}d_1^{opt} &= 1.286 - 3.704 \\ d_2^{opt} &= 0.422 - 2.689\end{aligned}$$

Of course,  $d_1^{opt}$  and/or  $d_2^{opt}$  could move outside of these ranges if any one or more of  $R_s$ ,  $\tau_m$ , and  $C_A$  exceed the limits used for these tables.

In those cases, Equations (16) and (17) could be used to compute exactly the optimal step durations for any combination of  $R_s$ ,  $\tau_m$ , and  $C_A$ .

- 5 In another embodiment, the device could also determine  $d_1^{opt}$  and  $d_2^{opt}$  based on measured values for  $R_s$ , and/or a programmed value for  $\tau_m$ , based on a particular value for  $C_A$  and  $C_B$ .

By way of example, if the capacitance value for  $C_A$  and  $C_B$  is set to 60  $\mu F$ , so that Equation 19 is satisfied for a tissue resistance,  $R_s$  equal to  
10 nominally 50 ohms and a tissue time constant,  $\tau_m$ , then for a range for  $\tau_m$ , of 2 ms to 4 ms, and a range for  $R_s$  of 30-90 ohms, then:

If  $\tau_m = 2.0$  ms and  $R_s = 90$  ohms, then:

$$(C_A + C_B) * R_s / \tau_m = 5.4$$

$$d_1^{opt} = 0.962 * \tau_m (= 1.923 \text{ ms})$$

15  $d_2^{opt} = 0.809 * \tau_m (= 1.618 \text{ ms})$

If  $\tau_m = 4.0$  ms and  $R_s = 30$  ohms, then:

$$(C_A + C_B) * R_s / \tau_m = 0.9$$

$$d_1^{opt} = 0.643 * \tau_m (= 2.573 \text{ ms})$$

20  $d_2^{opt} = 0.211 * \tau_m (= 0.844 \text{ ms})$

To further assist with interpreting the results embodied in **FIGS. 13 and 14** and the table shown in **FIGS. 15-17, FIG. 18** graphs a subset of those data as simple functions of  $R_s$  and  $\tau_m$ . In particular, **FIG. 18**  
25 presents a pair of graphs: the left and right halves plot  $d_1^{opt}$  and  $d_2^{opt}$ , respectively, as functions of  $R_s$  for three representative values of  $\tau_m$  (2, 3, and 4 ms). For these graphs,  $C_A = C_B = 60 \mu F$  (thus  $k = 1.0$ ). Consistent with the data in the tables shown in **FIGS. 15-17** both  $d_1^{opt}$  and  $d_2^{opt}$  increase in value with increasing  $R_s$  or  $\tau_m$ . Moreover, this figure helps

illustrate how  $d_1^{opt}$  appears significantly more sensitive to relative changes in  $\tau_m$  than in  $R_s$ , while  $d_2^{opt}$  appears to have the opposite sensitivity.

While **FIGS. 12-17** provide a comprehensive overview of all possible parallel-series two-step waveforms, it is also useful to consider some specific examples that can aid in illustrating the relative improvements gained by using such a parallel-series two-step capacitor arrangement over the traditional one-step arrangement.

**FIG. 19** graphically compares the positive portion of the biphasic shock waveform shapes ( $V_s$ , top two waveforms, 150 and 160) and associated tissue responses ( $V_m$ , bottom two waveforms, 152 and 162) for one-step, 150, and parallel-series two-step, 160, shocks having equal stored energies and leading-edge voltages.

For this example, shown in **FIG. 19**:

$$\tau_m = 3 \text{ ms}, R_s = 50 \text{ } \Omega, C_A = C_B = 60 \text{ } \mu\text{F}$$

(thus, Equations 15 & 19 are satisfied).

The one-step shock is generated by essentially keeping  $C_A$  and  $C_B$  in a parallel arrangement for its entire shock duration, for a constant effective capacitance of  $120 \text{ } \mu\text{F}$ . As is evident from the tissue responses (i.e., comparing the one-step response 152 to the two-step response 162), two-step the myocardial voltage (162) reaches a higher final cell membrane potential (+18.6%) in a shorter total duration (3.65 vs. 4.16 ms  $\Rightarrow$  - 12.3%) as compared to the final cell membrane potential (152) using the one-step shock. A consequence of this improved tissue response is that this two-step waveform requires a lower effective leading-edge voltage (and hence a lower stored energy) to achieve the same defibrillation efficacy as its equivalent one-step waveform.

**FIG. 20** illustrates this scenario by rescaling the results presented in **FIG. 19** such that the strength of each shock is sufficient to produce tissue responses of equal amplitudes. Consistent with the results presented in **FIG. 19**, this two-step positive portion of the biphasic shock waveform 164 theoretically requires a 15.6% lower leading-edge voltage than its one-step counterpart 154, which translates into a 28.8% reduction in required stored energy, and a potentially lower pain waveform for the patient since the leading edge of the shocking pulse is reduced.

**FIGS. 21 and 22** illustrate analogous results to those depicted in **FIG. 20**, but for relatively extreme combinations of  $R_s$  and  $C_A$ . In **FIG. 21**,  $R_s = 30\ \Omega$  and  $C_A = C_B = 30\ \mu\text{F}$ , while in **FIG. 22**,  $R_s = 90\ \Omega$  and  $C_A = C_B = 90\ \mu\text{F}$ . As is evident in **FIGS. 21 and 22**, the shape of the optimal parallel-series two-step waveform depends strongly on the magnitudes of  $R_s$  and  $C_A$ . Furthermore, the relative improvement in energy efficiency also strongly depends on these values.

For example, in **FIG. 21**, the two-step waveform 166 induced an equivalent final tissue response as its one-step waveform 156, but with an 8.8% shorter duration (2.1 vs. 2.3 ms), a 6.5% lower leading-edge voltage, and a 12.6% reduction in required stored energy.

In **FIG. 22**, the relative improvements were a 14.3% shorter duration (5.3 vs. 6.3 ms), a 25.9% lower leading-edge voltage, and a 45.0% reduction in required stored energy. Thus, these comparisons suggest that there would be especially great incentive for utilizing two-step waveforms instead of traditional one-step waveforms when the magnitudes of  $R_s$  and  $C_A$  are large, while the incentive is relatively minimal when the magnitudes of  $R_s$  and  $C_A$  are small. Unfortunately, because of the inherent limitations of this theoretical model, it is not possible to directly compare amplitude-based results (*e.g.*, leading-edge voltage, required stored energy) derived for differing  $R_s$  or  $\tau_m$ . For this

reason, the results of **FIGS. 20-22** are all self-normalized (that is, there is no relationship between the amplitudes in these graphs).

Finally, while Equations (16) and (17) provide exact formulas for determining  $d_1^{opt}$  and  $d_2^{opt}$  when  $k = 1$  (i.e.,  $C_A = C_B$ ), it is sometimes

5 helpful and/or practical to also identify various approximations to such solutions. Consider the following infinite series expansion of the natural logarithm:

$$\ln[x] = 2 \cdot \left[ \left( \frac{x-1}{x+1} \right) + \frac{1}{3} \cdot \left( \frac{x-1}{x+1} \right)^3 + \frac{1}{5} \cdot \left( \frac{x-1}{x+1} \right)^5 + \dots \right] \quad (x > 0) \quad (\text{Eq. 23})$$

Utilizing just the first term of this expansion, Equations (16) and (17) can

10 be simplified to:

$$\begin{aligned} d_1^{opt} &\approx \frac{2\tau_m}{3 - \alpha_1} = \frac{2\tau_{s1} \cdot \tau_m}{2\tau_{s1} + \tau_m} \Rightarrow \frac{1}{d_1^{opt}} \approx \frac{1}{2\tau_{s1}} + \frac{1}{\tau_m} = \frac{1}{4R_s C_A} + \frac{1}{\tau_m} \\ d_2^{opt} &\approx \frac{2\tau_m}{3 - 2\alpha_2} = \frac{\tau_{s2} \cdot 2\tau_m}{\tau_{s2} + 2\tau_m} \Rightarrow \end{aligned} \quad (\text{Eq. 24})$$

$$15 \quad \frac{1}{d_2^{opt}} \approx \frac{1}{\tau_{s2}} + \frac{1}{2\tau_m} = \frac{1}{2} \cdot \left( \frac{4}{R_s C_A} + \frac{1}{\tau_m} \right) \quad (\text{Eq. 25})$$

In words, these relationships suggest that the optimal step durations can be well approximated by computing variously weighted *parallel* combinations of system and myocardial time constants. And despite using only one term of Equation (23), these approximations are

20 relatively quite accurate over a broad range of  $\tau_{s1}/\tau_m$  and  $\tau_{s2}/\tau_m$  ratios (only their ratios, not their absolute values, impact their accuracy). For example, the relative error for  $d_1^{opt}$  is less than 5% for  $0.4 < \tau_{s1}/\tau_m < 5$ , while the relative error for  $d_2^{opt}$  is less than 5% for  $0.2 < \tau_{s2}/\tau_m < 3$ . When

25 Equation (20) is also satisfied (that is, when system and myocardial time constants are ideally matched), these relative errors are each only 1.35%.

In all cases, these approximation calculations underestimate the true values by these respective relative errors.

Optimal Three-Step Positive Phase Pulse Generation

In the forgoing, techniques for generating two- and three-step biphasic shocking pulses have been described wherein the first (typically positive) phase of the biphasic pulse has no more than two voltage peaks. In the following, techniques will be described for generating a biphasic shocking pulse wherein the positive phase of the pulse has three distinct voltage peaks. Pulse 200, illustrated in **FIG. 23**, is generated using the three-capacitor circuit of **FIG. 4**, but controlled so as to generate a biphasic pulse having a positive phase containing three distinct voltage peaks. (In **FIG. 23**, only the positive phase of the biphasic pulse is shown.) The three capacitors are discharged as follows: a first step or portion 202 of the pulse waveform is generated by discharging capacitors C1, C2, and C3 while all three are connected in parallel for a time period of  $d_1$ ; a second step 204 of the pulse waveform is generated by discharging the capacitors while the C1 and C2 are connected in parallel and C3 is connected in series for a time period of  $d_2$ ; and a third step 206 of the pulse waveform by discharging the capacitors while all three are connected in series for a time period of  $d_3$ . The duration of each phase is selected to maximize the final myocardial voltage within the heart tissue receiving the pulse. To this end, the initial voltage of each capacitor is set to  $V_0$  and the optimal time durations for each phase of the pulse are as follows:

$$d_1^{opt} = -\frac{\tau_m}{\alpha_1} \cdot \ln \left\{ \left( \frac{\tau_m}{\tau_{s1}} \right) \left( \frac{2 - \frac{\alpha_2}{\alpha_1}}{1 - \frac{\alpha_2}{\alpha_1}} \right) \right\}; \quad (\text{Eq. 26})$$

$$d_2^{opt} = +\frac{\tau_m}{\alpha_2} \cdot \ln \left\{ \left( \frac{1}{2} \right) \left( \frac{2 - \frac{\alpha_2}{\alpha_1}}{1 - \frac{\alpha_2}{\alpha_1}} \right) \left( \frac{1 - \frac{\alpha_3}{\alpha_2}}{K_C - \frac{\alpha_3}{\alpha_2}} \right) \right\}; \text{ and} \quad (\text{Eq. 27})$$

$$d_3^{opt} = -\frac{\tau_m}{\alpha_3} \cdot \ln \left\{ \left( K_C \right) \frac{1 - \frac{\alpha_3}{\alpha_2}}{K_C - \frac{\alpha_3}{\alpha_2}} \right\} \quad (\text{Eq. 28})$$

In the Equations (26) - (28),

$$K_C = 1 + (C_C) / (C_A + C_B + C_C); \quad (\text{Eq. 29})$$

$$\alpha_1 = 1 - (\tau_m / \tau_{s1}), \quad \alpha_2 = 1 - (\tau_m / \tau_{s2}), \quad \text{and} \quad \alpha_3 = 1 - (\tau_m / \tau_{s3}); \quad (\text{Eq. 30})$$

$$\tau_{s1} = R_s \cdot C_{s1}; \quad \tau_{s2} = R_s \cdot C_{s2}; \quad \text{and} \quad \tau_{s3} = R_s \cdot C_{s3}; \quad (\text{Eq. 31})$$

$$C_{s1} = C_A + C_B + C_C; \quad (\text{Eq. 32})$$

$$C_{s2} = [(C_A + C_B) \cdot (C_C)] / [C_A + C_B + C_C]; \quad (\text{Eq. 33})$$

$$C_{s3} = 1 / \left[ \frac{1}{C_A} + \frac{1}{C_B} + \frac{1}{C_C} \right] \quad (\text{Eq. 34})$$

$C_A$ ,  $C_B$ , &  $C_C$  are the capacitances, respectively, of the first, second and third capacitors C1, C2 and C3; and

$\tau_m$  is a predetermined myocardial tissue time constant.

Note that  $C_A$ ,  $C_B$ , &  $C_C$  are the capacitances of the capacitors C1, C2 and C3 of the three capacitor system of **FIG. 4** and should not be confused with the capacitances of capacitors  $C_A$ ,  $C_B$  of the two capacitor system of **FIG. 3**. To clarify, all references herein to  $C_A$ ,  $C_B$ , &  $C_C$  within the equations of the Summary, the Claims, **FIGS. 23** and following and Equations 26 and following refer to the capacitances of the capacitors C1, C2 and C3 of the three capacitor system of **FIG. 4**.

Preferably, the capacitances of the three capacitors are selected so as to minimize the amount of required stored energy while achieving the maximum final myocardial voltage. To minimize the amount of required stored energy, the capacitances are set to:

$$C_A^{opt} = 0.6673 \cdot \left( \frac{\tau_m}{R_s} \right); \quad (\text{Eq. 35})$$



$$C_B^{opt} = 0.6673 \cdot \left( \frac{\tau_m}{R_s} \right); \text{ and} \quad (\text{Eq. 36})$$

$$C_C^{opt} = 1.5356 \cdot \left( \frac{\tau_m}{R_s} \right); \text{ wherein} \quad (\text{Eq. 37})$$

$R_s$  is a predetermined system resistance.

By using the optimal capacitance values, the optimal discharge  
5 time periods  $d_1^{opt}$ ,  $d_2^{opt}$ , and  $d_3^{opt}$  for use in maximizing the myocardial  
potential may be simplified to:

$$d_1^{opt} = 0.878 \cdot \tau_m; \quad (\text{Eq. 38})$$

$$d_2^{opt} = 0.277 \cdot \tau_m; \text{ and} \quad (\text{Eq. 39})$$

$$d_3^{opt} = 0.200 \cdot \tau_m. \quad (\text{Eq. 40})$$

10

Description	Var	Value	Optimal	Units
System resistance	Rs	50.0		ohms
Myocardial time constant	$\tau_m$	3.00		ms
Capacitor A	CA	40.0	<b>40.0</b>	$\mu\Phi$
Capacitor B	CB	40.0	<b>40.0</b>	$\mu\Phi$
Capacitor C	CC	92.1	<b>92.1</b>	$\mu\Phi$
Total Capacitance	Ctotal	172.2	<b>172.2</b>	$\mu\Phi$

TABLE I

Derived Intermediate Values			
Description	Var	Value	Units
Step1 time constant	$\tau\sigma_1$	8.61	ms
Step2 time constant	$\tau\sigma_2$	2.14	ms
Step3 time constant	$\tau\sigma_3$	0.82	ms
alpha1	$\alpha_1$	0.65	none
alpha2	$\alpha_2$	-0.40	none
alpha3	$\alpha_3$	-2.65	none

TABLE II

Optimal Values				
Description	Var	Value	Units	
Optimal Step1 duration	d1	2.64	ms	
Optimal Step2 duration	d2	0.83	ms	
Optimal Step3 duration	d3	0.60	ms	
Total duration	Dtotal	4.07	ms	
Step1 leading-edge voltage	V01	1.00	1.35	
Step2 leading-edge voltage	V02	1.47	1.99	
Step3 leading-edge voltage	V03	1.53	2.07	(rel units)
Step1 myo. final voltage	Vm1f	0.49	0.67	
Step2 myo. final voltage	Vm2f	0.67	0.90	
Step3 myo. final voltage	Vm3f	0.74	1.00	(rel units)

TABLE III

By configuring and operating the three capacitor shocking circuit as just summarized, the amount of energy required to reach a myocardial defibrillation threshold is less than for one-capacitor or two-capacitor systems, regardless of the total capacitance of the system. Hence, power can be saved, while still providing effective defibrillation. Moreover, the total time required to reach the myocardial defibrillation threshold is less than with one-capacitor or two-capacitor systems, permitting the patient to be defibrillated more quickly. Additionally, using the three capacitor system to generate pulses having a three-step positive phase is generally less influenced by variations in underlying parameters and operating conditions, than one- or two-capacitor arrangements.

In view of the foregoing, a method for making and using an ICD exploiting an optimal three-step positive -phase shocking pulse may be exploited. The method is summarized in **FIG. 26**. Initially, at step 250, the system resistance  $R_s$  (as seen by the shocking circuit) and the myocardial tissue time constant  $\tau_m$  are determined by conventional techniques. Then, at step 252, the optimal capacitance values for the three capacitors are determined using Equations (35) - (37). At step 254,

the optimal discharge time values for the three phases of the pulse waveform are determined using Equations (38) - (40). An ICD is then fabricated, at step 256, with shocking circuit capacitors having the optimal capacitances and programmed to discharge the capacitors for the optimal time periods. The ICD is then implanted within a patient at step 258 and is activated to detect ventricular fibrillation. The capacitors are charged to a selected voltage. Upon detection of fibrillation, at step 260, the ICD discharges the capacitors using the sequence described above to deliver a three-step positive phase of the shocking pulse to the patient for terminating fibrillation. If the first pulse fails to terminate fibrillation, additional pulses may be delivered, perhaps using higher voltage levels. Note that, if it is not practicable to provide an ICD with capacitors exactly matching the optimal capacitance values, approximate values may be employed instead. If so, then values for the discharge time periods are calculated for use with the actual capacitance values using Equations (26) - (28), and the ICD is programmed accordingly.

Table IV provides a summary of the parameters for the three distinct steps of the waveform:

<b>Step1</b>	Capacitor Arrangement	$C_A, C_B, \text{ and } C_C \text{ in parallel}$
	Effective Capacitance	$C_{s1} = C_A + C_B + C_C$
	Decay Time Constant	$\tau_{s1} = R_s \cdot C_{s1}$
	Leading Edge Voltage	$V_{01} = V_0$
	Total Voltage Profile	$V_{s1}(t_1) = V_{01} \cdot \exp[-t_1/\tau_{s1}] \quad 0 \leq t_1 \leq d_1$
<b>Step2</b>	Capacitor Arrangement	$C_A \text{ and } C_B \text{ in parallel, } C_C \text{ in series}$
	Effective Capacitance	$C_{s2} = [(C_A + C_B) \cdot (C_C)] / [C_A + C_B + C_C]$
	Decay Time Constant	$\tau_{s2} = R_s \cdot C_{s2}$
	Leading Edge Voltage	$V_{02} = 2 \cdot V_{s1}(d_1)$ $= 2 \cdot V_0 \cdot \exp[-d_1/\tau_{s1}]$
	Total Voltage Profile	$V_{s2}(t_2) = V_{02} \cdot \exp[-t_2/\tau_{s2}] \quad 0 \leq t_2 \leq d_2$
<b>Step3</b>	Capacitor Arrangement	$C_A, C_B, \text{ and } C_C \text{ in series}$
	Effective Capacitance	$C_{s3} = 1 / \left[ \frac{1}{C_A} + \frac{1}{C_B} + \frac{1}{C_C} \right]$
	Decay Time Constant	$\tau_{s3} = R_s \cdot C_{s3}$
	Leading Edge Voltage	$V_{03} = K_C \cdot V_{s2}(d_2)$ $= 2 \cdot K_C \cdot V_0 \cdot \exp[-d_1/\tau_{s1}] \cdot \exp[-d_2/\tau_{s2}]$  $\text{where } K_C = 1 + \frac{C_C}{C_A + C_B + C_C}$
	Total Voltage Profile	$V_{s3}(t_3) = V_{03} \cdot \exp[-t_3/\tau_{s3}]$ $0 \leq t_3 \leq d_3$

TABLE IV

The aforementioned optimal pulse phase durations and capacitance values have been derived as follows. The defibrillation waveform is represented by:

$$V_{s1}(t_1) = V_{01} \cdot \exp[-t_1/\tau_{s1}] \quad 0 \leq t_1 \leq d_1 \quad (\text{Eq. 41})$$

$$V_{s2}(t_2) = V_{02} \cdot \exp[-t_2/\tau_{s2}] \quad 0 \leq t_2 \leq d_2 \quad (\text{Eq. 42})$$

$$V_{s3}(t_3) = V_{03} \cdot \exp[-t_3/\tau_{s3}] \quad 0 \leq t_3 \leq d_3 \quad (\text{Eq. 43})$$

A General Solution for  $V_m(t)$  is obtained with the following derivations. Note that the following derivations (Equations (44) - (46)) make no assumptions regarding any specific relationships between the characteristics of Step1, Step2, and Step3.

The idealized myocardial responses ( $V_{m1}$ ,  $V_{m2}$ , and  $V_{m3}$ ) to the three steps of the applied waveform ( $V_{s1}$ ,  $V_{s2}$ , and  $V_{s3}$ ) can be described as the solution to the following set of sequential equations:

$$\text{Step1: } \frac{V_{s1}(t_1)}{\tau_m} = \frac{dV_{m1}(t_1)}{dt_1} + \frac{V_{m1}(t_1)}{\tau_m} \quad (\text{Eq. 44})$$

$$\text{Step2: } \frac{V_{s2}(t_2)}{\tau_m} = \frac{dV_{m2}(d_1, t_2)}{dt_2} + \frac{V_{m2}(d_1, t_2)}{\tau_m} \quad (\text{Eq. 45})$$

$$\text{Step3: } \frac{V_{s3}(t_3)}{\tau_m} = \frac{dV_{m3}(d_1, d_2, t_3)}{dt_3} + \frac{V_{m3}(d_1, d_2, t_3)}{\tau_m} \quad (\text{Eq. 46})$$

with the corresponding set of initial conditions given as:  $V_{m1}(0) = 0$ ,  $V_{m2}(d_1, 0) = V_{m1}(d_1)$ , and  $V_{m3}(d_1, d_2, 0) = V_{m2}(d_1, d_2)$ . The initial conditions specify that the myocardial voltage is initially at a voltage level of zero,

and furthermore that the myocardial voltage must be continuous between consecutive steps.

The corresponding general solutions to these differential equations are:

5 Step1:

$$V_{m1}(t_1) = \frac{V_{01}}{\alpha_1} \cdot \left( \exp\left[\frac{-t_1}{\tau_{s1}}\right] - \exp\left[\frac{-t_1}{\tau_m}\right] \right) \quad \tau_{s1} \neq \tau_m \quad (\text{Eq. 46})$$

Step2:

$$\begin{aligned} V_{m2}(d_1, t_2) = & V_{m1}(d_1) \cdot \exp\left[\frac{-t_2}{\tau_m}\right] \\ & + \frac{V_{02}}{\alpha_2} \cdot \left( \exp\left[\frac{-t_2}{\tau_{s2}}\right] - \exp\left[\frac{-t_2}{\tau_m}\right] \right) \quad \tau_{s2} \neq \tau_m \end{aligned} \quad (\text{Eq. 47})$$

Step3:

$$\begin{aligned} V_{m3}(d_1, d_2, t_3) = & V_{m2}(d_1, d_2) \cdot \exp\left[\frac{-t_3}{\tau_m}\right] \\ & + \frac{V_{03}}{\alpha_3} \cdot \left( \exp\left[\frac{-t_3}{\tau_{s3}}\right] - \exp\left[\frac{-t_3}{\tau_m}\right] \right) \quad \tau_{s3} \neq \tau_m \end{aligned} \quad (\text{Eq. 48})$$

where  $\alpha_1 = 1 - (\tau_m / \tau_{s1})$ ,  $\alpha_2 = 1 - (\tau_m / \tau_{s2})$ , and  $\alpha_3 = 1 - (\tau_m / \tau_{s3})$ .

(The associated solutions for when  $\tau_{s1} = \tau_m$ ,  $\tau_{s2} = \tau_m$ , or  $\tau_{s3} = \tau_m$  are straightforward, but not relevant to these derivations, and thus are not included here.)

15

One of the main objectives of these derivations is to find the combination of waveform step durations that will maximize the final myocardial response. This goal corresponds to finding the step durations,  $d_1=d_1^{opt}$ ,  $d_2=d_2^{opt}$ , and  $d_3=d_3^{opt}$ , that maximize the final

- 5 myocardial voltage given by  $V_{m3}(t_1=d_1, t_2=d_2, t_3=d_3)$ . This maximum can be determined by solving for these step durations from the following simultaneous equations:

$$\frac{\partial V_{m3}(d_1^{opt}, d_2^{opt}, d_3^{opt})}{\partial d_1^{opt}} = 0 \quad (\text{Eq. 49})$$

$$\frac{\partial V_{m3}(d_1^{opt}, d_2^{opt}, d_3^{opt})}{\partial d_2^{opt}} = 0 \quad (\text{Eq. 50})$$

10 
$$\frac{\partial V_{m3}(d_1^{opt}, d_2^{opt}, d_3^{opt})}{\partial d_3^{opt}} = 0 \quad (\text{Eq. 51})$$

Given the relationships and definitions presented in the table above, the solutions to this set of equations are:

$$d_1^{opt} = -\frac{\tau_m}{\alpha_1} \cdot \ln \left\{ \left( \frac{\tau_m}{\tau_{s1}} \right) \left( \frac{2 - \frac{\alpha_2}{\alpha_1}}{1 - \frac{\alpha_2}{\alpha_1}} \right) \right\} \quad (\text{Eq. 52})$$

$$d_2^{opt} = +\frac{\tau_m}{\alpha_2} \cdot \ln \left\{ \left( \frac{1}{2} \right) \left( \frac{2 - \frac{\alpha_2}{\alpha_1}}{1 - \frac{\alpha_2}{\alpha_1}} \right) \left( \frac{1 - \frac{\alpha_3}{\alpha_2}}{K_C - \frac{\alpha_3}{\alpha_2}} \right) \right\} \quad (\text{Eq. 53})$$

15 
$$d_3^{opt} = -\frac{\tau_m}{\alpha_3} \cdot \ln \left\{ \left( K_C \right) \left( \frac{1 - \frac{\alpha_3}{\alpha_2}}{K_C - \frac{\alpha_3}{\alpha_2}} \right) \right\} \quad (\text{Eq. 54})$$

where  $K_C = 1 + (C_C)/(C_A + C_B + C_C)$ .

Note that Equations (52) - (54) define the optimal step durations that maximize final myocardial voltage for *any independent values* of  $C_A$ ,  $C_B$ , and  $C_C$ . However, since efficient use of stored energy is critically important for implantable defibrillators, it is desirable to determine the optimal values for the capacitors that maximizes induced myocardial voltage while minimizing required stored energy. Considering the complexity of the governing equations involved in this optimization problem, finding these capacitor values is best performed numerically using conventional nonlinear optimization techniques. The results are presented in Table V, where the optimal values for the capacitors are defined as functions of the governing ratio ( $\tau_m/R_s$ ):

	$C_A^{opt}$	$C_B^{opt}$	$C_C^{opt}$	$C_{total}^{opt}$
<i>Exact Values</i>	$0.6673 \cdot \left(\frac{\tau_m}{R_s}\right)$	$0.6673 \cdot \left(\frac{\tau_m}{R_s}\right)$	$1.5356 \cdot \left(\frac{\tau_m}{R_s}\right)$	$2.8701 \cdot \left(\frac{\tau_m}{R_s}\right)$
<i>Approx Values</i>	$\left(\frac{2}{3}\right) \cdot \left(\frac{\tau_m}{R_s}\right)$	$\left(\frac{2}{3}\right) \cdot \left(\frac{\tau_m}{R_s}\right)$	$\left(\frac{3}{2}\right) \cdot \left(\frac{\tau_m}{R_s}\right)$	$\left(\frac{17}{6}\right) \cdot \left(\frac{\tau_m}{R_s}\right)$
<i>Relative Error</i>	-0.09%	-0.09%	-2.32%	-1.28%

TABLE V

Thus, for example, with  $\tau_m = 3$  ms and  $R_s = 50 \Omega$ , the optimal values for  $C_A$ ,  $C_B$ , and  $C_C$  are 40.036, 40.036, and 92.136  $\mu\text{F}$ , respectively, for a total optimal capacitance of 172.208  $\mu\text{F}$ . For comparison, the capacitance values obtained by using the approximating expressions above are 40, 40, and 90  $\mu\text{F}$ , respectively, for a total of 170  $\mu\text{F}$ .

If (and only if) optimal capacitance values (as obtained from the Table above) are utilized as appropriate for the governing system conditions (*i.e.*, the specific values of  $\tau_m$  and  $R_s$ ), then Equations (52)–(54) can be simplified dramatically as follows:

$$d_1^{opt} = 0.878 \cdot \tau_m \quad (\text{Eq. 55})$$



$$d_2^{opt} = 0.277 \cdot \tau_m \quad (\text{Eq. 56})$$

$$d_3^{opt} = 0.200 \cdot \tau_m \quad (\text{Eq. 57})$$

Based on the algebraic expressions for optimal capacitance values (as a function of  $\tau_m/R_s$ ) as given in the Table above, the normalized sizes of the capacitors  $C_A$ ,  $C_B$ , and  $C_C$  relative to the total optimal capacitance can be derived as follows:

$$C_A^{opt} / C_{total}^{opt} = C_B^{opt} / C_{total}^{opt} = 0.2325$$

$$C_C^{opt} / C_{total}^{opt} = 0.5350$$

Note that these ratios are not completely invariant to deviations from optimal. That is, the ratios cannot always be employed to calculate the most appropriate individual capacitor values for *any* given total capacitance (e.g.,  $C_{total} \neq C_{total}^{opt}$ ). However, the ratios have been found to be quite usable over a broad range of excursions from optimal. As **FIG. 27** illustrates, the individual-to-total capacitance ratios do vary slightly as the actual total capacitance diverges from the optimal total capacitance (i.e.,  $C_{total}/C_{opt} \neq 1$ ). However, since these ratio variations are relatively insensitive to these excursions (only 0.79% and 1.58% change in  $C_A/C_{total}$  and  $C_C/C_{total}$ , respectively, per unit change in  $C_{total}/C_{opt}$ ), the ratios above are quite satisfactory for most purposes (and can be adjusted by these percentage deviations to provide even further accuracy, if needed).

A comparison of three-capacitor results to those from one-capacitor and two-capacitor systems follows below. Firstly, the results above imply that the *total* system capacitance for an optimally configured three-capacitor defibrillator is almost  $3 \cdot (\tau_m/R_s)$  [the actual coefficient, as indicated in the Table V above, equals 2.8701]. For comparison, the total system capacitance for an optimally configured two-capacitor two-step parallel-series defibrillator (as determined from a previously completed

set of derivations) equals exactly  $2 \cdot (\tau_m/R_s)$ , with those two capacitors equal in magnitude. Moreover, the total system capacitance for an optimally configured one-capacitor one-step defibrillator equals only  $1 \cdot (\tau_m/R_s)$ . Thus, the total system capacitance for a three-capacitor defibrillator as recommended from these (idealized) derivations is actually significantly larger than the simpler system designs. However, as will be explained with reference to the remaining figures, the required stored energy is less, the time to defibrillation threshold is faster, and the three-capacitor system is less influenced by underlying parameters and operating conditions.

**FIG. 28** plots the relative total stored energy as a function of total capacitance theoretically required to reach the “defibrillation” threshold ( $V_{th}$ ) for an idealized myocardial tissue model for exemplary one-capacitor, two-capacitor, and three-capacitor systems. In this example,  $\tau_m = 3$  ms and  $R_s = 50 \Omega$ ; for other combinations of  $\tau_m$  and  $R_s$ , the quantitative aspects of this plot will change, but the qualitative relationships are not be affected. The drop-arrows superimposed in the figure indicate the total capacitance values at which the energy curves reach their respective minima; these total capacitance values thus also indicate the optimal total capacitances for these particular capacitor configurations (*i.e.*, 60, 120, and 172.2  $\mu$ F for the one-capacitor, two-capacitor, and three-capacitor configurations, respectively, at the specific values of  $\tau_m$  and  $R_s$ ). As the graph further illustrates, while the optimal total capacitance of the three-capacitor configuration is greater than either of the simpler configurations, the relative stored energy it requires to reach threshold is significantly less than that needed for either one-capacitor or two-capacitor configurations across all values of total capacitance. For any fixed total capacitance, the largest relative reduction in energy requirements occurs when moving from the one-capacitor to two-capacitor configurations, although additional marginal energy savings are indeed realized by moving to the three-capacitor

configuration. Table VI summarizes and compares these results for the selected set of data points associated with the drop-arrows on **FIG. 28** (all stored energies are normalized by the minimum value from the three-capacitor configuration):

5

	Relative Stored Energy to reach $V_{th}$					
$C_{total}$	one- capacitor	two- capacitor	three- capacitor	2 vs 1	3 vs 1	3 vs 2
60	1.411	1.150	1.107	-18.5%	-21.6%	-3.7%
120	1.527	1.087	1.012	-28.8%	-33.8%	-7.0%
172.2	1.692	1.104	1.000	-34.8%	-40.9%	-9.4%

TABLE VI

Another important observation to be made from **FIG. 28** is that the energy profile from the three-capacitor configuration is significantly  
10 “flatter” as a function of total capacitance than that from either of the other configurations, indicating that the three-capacitor configuration is likely to be more robust to variations or drift in underlying parameters or operating conditions.

Beyond a reduction in required stored energy, another advantage  
15 realized by using a three-capacitor configuration is that the total shock duration necessary to reach myocardial threshold is likewise shorter than that required by a one-capacitor or two-capacitor configuration. **FIG. 29** illustrates this comparative advantage between the three-capacitor and one- and two-capacitor configurations based on the same system  
20 conditions used in **FIG. 28**. As expected, for all configurations, total shock duration is a monotonically increasing function of total system capacitance. However, the multi-step configurations are consistently shorter in duration than the simpler configurations. And, as with the relationship observed for total stored energy, for any fixed total  
25 capacitance, the largest relative reduction in total duration occurs when

moving from the one-capacitor to two-capacitor configurations, although additional marginal duration shortening is indeed realized by moving to the three-capacitor configuration.

Table VII summarizes and compares these duration results for the selected set of data points:

	Total Duration (ms) to reach $V_{th}$					
$C_{total}$	one-capacitor	Two-capacitor	three-capacitor	2 vs 1	3 vs 1	3 vs 2
60	3.00	2.69	2.64	— 10.23%	— 12.14%	— 2.13%
120	4.16	3.65	3.54	— 12.26%	— 14.86%	— 2.97%
172.2	5.73	5.01	4.86	— 12.46%	— 15.15%	— 3.08%

TABLE VII

#### Exemplary ICD design

The invention may be implemented in an ICD configured as follows. As shown in **FIG. 30**, there is a stimulation device 310 in electrical communication with a patient's heart 312 by way of three leads, 320, 324 and 330, suitable for delivering multi-chamber stimulation and shock therapy. To sense atrial cardiac signals and to provide right atrial chamber stimulation therapy, the stimulation device 310 is coupled to an implantable right atrial lead 320 having at least an atrial tip electrode 322, which typically is implanted in the patient's right atrial appendage.

To sense left atrial and ventricular cardiac signals and to provide left chamber pacing therapy, the stimulation device 310 is coupled to a "coronary sinus" lead 324 designed for placement in the "coronary sinus region" via the coronary sinus os for positioning a distal electrode adjacent to the left ventricle and/or additional electrode(s) adjacent to the left atrium. As used herein, the phrase "coronary sinus region" refers to the vasculature of the left ventricle, including any portion of the coronary

sinus, great cardiac vein, left marginal vein, left posterior ventricular vein, middle cardiac vein, and/or small cardiac vein or any other cardiac vein accessible by the coronary sinus.

Accordingly, an exemplary coronary sinus lead 324 is designed to receive atrial and ventricular cardiac signals and to deliver left ventricular pacing therapy using at least a left ventricular tip electrode 326, left atrial pacing therapy using at least a left atrial ring electrode 327, and shocking therapy using at least a left atrial coil electrode 328. For a complete description of a coronary sinus lead, and U.S. Patent No. 5,466,254, "Coronary Sinus Lead with Atrial Sensing Capability" (Helland), which patents are hereby incorporated herein by reference.

The stimulation device 310 is also shown in electrical communication with the patient's heart 312 by way of an implantable right ventricular lead 330 having, in this embodiment, a right ventricular tip electrode 332, a right ventricular ring electrode 334, a right ventricular (RV) coil electrode 336, and an SVC coil electrode 338. Typically, the right ventricular lead 330 is transvenously inserted into the heart 312 so as to place the right ventricular tip electrode 332 in the right ventricular apex so that the RV coil electrode will be positioned in the right ventricle and the SVC coil electrode 338 will be positioned in the superior vena cava. Accordingly, the right ventricular lead 330 is capable of receiving cardiac signals, and delivering stimulation in the form of pacing and shock therapy to the right ventricle.

As illustrated in **FIG. 30**, a simplified block diagram is shown of the multi-chamber implantable stimulation device 310, which is capable of treating both fast and slow arrhythmias with stimulation therapy, including cardioversion, defibrillation, and pacing stimulation. While a particular multi-chamber device is shown, this is for illustration purposes only, and one of skill in the art could readily duplicate, eliminate or disable the appropriate circuitry in any desired combination to provide a device

capable of treating the appropriate chamber(s) with cardioversion, defibrillation and pacing stimulation.

The housing 340 for the stimulation device 310, shown schematically in **FIG. 30**, is often referred to as the "can", "case" or "case electrode" and may be programmably selected to act as the return electrode for all "unipolar" modes. The housing 340 may further be used as a return electrode alone or in combination with one or more of the coil electrodes, 328, 36 and 38, for shocking purposes. The housing 340 further includes a connector (not shown) having a plurality of terminals, 342, 344, 346, 348, 352, 354, 356, and 358 (shown schematically and, for convenience, the names of the electrodes to which they are connected are shown next to the terminals). As such, to achieve right atrial sensing and pacing, the connector includes at least a right atrial tip terminal (A<sub>R</sub> TIP) 342 adapted for connection to the atrial tip electrode 322.

To achieve left chamber sensing, pacing and shocking, the connector includes at least a left ventricular tip terminal (V<sub>L</sub> TIP) 344, a left atrial ring terminal (A<sub>L</sub> RING) 346, and a left atrial shocking terminal (A<sub>L</sub> COIL) 348, which are adapted for connection to the left ventricular ring electrode 326, the left atrial tip electrode 327, and the left atrial coil electrode 328, respectively.

To support right chamber sensing, pacing and shocking, the connector further includes a right ventricular tip terminal (V<sub>R</sub> TIP) 352, a right ventricular ring terminal (V<sub>R</sub> RING) 354, a right ventricular shocking terminal (R<sub>V</sub> COIL) 356, and an SVC shocking terminal (SVC COIL) 358, which are adapted for connection to the right ventricular tip electrode 32, right ventricular ring electrode 334, the RV coil electrode 336, and the SVC coil electrode 338, respectively.

At the core of the stimulation device 310 is a programmable microcontroller 360 that controls the various modes of stimulation therapy. As is well known in the art, the microcontroller 360 typically includes a microprocessor, or equivalent control circuitry, designed

specifically for controlling the delivery of stimulation therapy and may further include RAM or ROM memory, logic and timing circuitry, state machine circuitry, and I/O circuitry. Typically, the microcontroller 360 includes the ability to process or monitor input signals (data) as controlled  
5 by a program code stored in a designated block of memory. The details of the design and operation of the microcontroller 360 are not critical to the present invention. Rather, any suitable microcontroller 360 may be used that carries out the functions described herein. The use of microprocessor-based control circuits for performing timing and data  
10 analysis functions are well known in the art.

As shown in **FIG. 30**, an atrial pulse generator 370 and a ventricular pulse generator 372 generate pacing stimulation pulses for delivery by the right atrial lead 320, the right ventricular lead 330, and/or the coronary sinus lead 324 via an electrode configuration switch 374. It  
15 is understood that in order to provide stimulation therapy in each of the four chambers of the heart, the atrial and ventricular pulse generators, 370 and 372, may include dedicated, independent pulse generators, multiplexed pulse generators, or shared pulse generators. The pulse generators, 370 and 372, are controlled by the microcontroller 360 via  
20 appropriate control signals, 376 and 378, respectively, to trigger or inhibit the stimulation pulses.

The microcontroller 360 further includes timing control circuitry 379 which is used to control the timing of such stimulation pulses (e.g., pacing rate, atrio-ventricular (AV) delay, atrial interconduction (A-A) delay, or  
25 ventricular interconduction (V-V) delay, etc.) as well as to keep track of the timing of refractory periods, PVARP intervals, noise detection windows, evoked response windows, alert intervals, marker channel timing, etc., which is well known in the art.

The switch 374 includes a plurality of switches for connecting the  
30 desired electrodes to the appropriate I/O circuits, thereby providing complete electrode programmability. Accordingly, the switch 374, in

response to a control signal 380 from the microcontroller 360, determines the polarity of the stimulation pulses (e.g., unipolar, bipolar, combipolar, etc.) by selectively closing the appropriate combination of switches (not shown) as is known in the art.

5           Atrial sensing circuits 382 and ventricular sensing circuits 384 may also be selectively coupled to the right atrial lead 320, coronary sinus lead 324, and the right ventricular lead 330, through the switch 374 for detecting the presence of cardiac activity in each of the four chambers of the heart. Accordingly, the atrial (ATR. SENSE) and ventricular (VTR.  
10       SENSE) sensing circuits, 382 and 384, may include dedicated sense amplifiers, multiplexed amplifiers, or shared amplifiers. The switch 374 determines the "sensing polarity" of the cardiac signal by selectively closing the appropriate switches, as is also known in the art. In this way, the clinician may program the sensing polarity independent of the  
15       stimulation polarity.

Each sensing circuit, 382 and 384, preferably employs one or more low power, precision amplifiers with programmable gain and/or automatic gain control, bandpass filtering, and a threshold detection circuit, as known in the art, to selectively sense the cardiac signal of interest. The  
20       automatic gain control enables the device 310 to deal effectively with the difficult problem of sensing the low amplitude signal characteristics of atrial or ventricular fibrillation. The outputs of the atrial and ventricular sensing circuits, 382 and 384, are connected to the microcontroller 360 which, in turn, are able to trigger or inhibit the atrial and ventricular pulse  
25       generators, 370 and 372, respectively, in a demand fashion in response to the absence or presence of cardiac activity in the appropriate chambers of the heart.

For arrhythmia detection, the device 310 utilizes the atrial and ventricular sensing circuits, 382 and 384, to sense cardiac signals to  
30       determine whether a rhythm is physiologic or pathologic. As used herein "sensing" is reserved for the noting of an electrical signal, and "detection"



is the processing of these sensed signals and noting the presence of an arrhythmia. The timing intervals between sensed events (e.g., P-waves, R-waves, and depolarization signals associated with fibrillation which are sometimes referred to as "F-waves" or "Fib-waves") are then classified by the microcontroller 360 by comparing them to a predefined rate zone limit (i.e., bradycardia, normal, low rate VT, high rate VT, and fibrillation rate zones) and various other characteristics (e.g., sudden onset, stability, physiologic sensors, and morphology, etc.) in order to determine the type of remedial therapy that is needed (e.g., bradycardia pacing, anti-tachycardia pacing, cardioversion shocks or defibrillation shocks, collectively referred to as "tiered therapy").

Cardiac signals are also applied to the inputs of an analog-to-digital (A/D) data acquisition system 390. The data acquisition system 390 is configured to acquire intracardiac electrogram signals, convert the raw analog data into a digital signal, and store the digital signals for later processing and/or telemetric transmission to an external device 402. The data acquisition system 390 is coupled to the right atrial lead 320, the coronary sinus lead 324, and the right ventricular lead 330 through the switch 374 to sample cardiac signals across any pair of desired electrodes.

The microcontroller 360 is further coupled to a memory 394 by a suitable data/address bus 396, wherein the programmable operating parameters used by the microcontroller 360 are stored and modified, as required, in order to customize the operation of the stimulation device 310 to suit the needs of a particular patient. Such operating parameters define, for example, pacing pulse amplitude, pulse duration, electrode polarity, rate, sensitivity, automatic features, arrhythmia detection criteria, and the amplitude, waveshape and vector of each shocking pulse to be delivered to the patient's heart 312 within each respective tier of therapy.

Advantageously, the operating parameters of the implantable device 310 may be non-invasively programmed into the memory 394

through a telemetry circuit 400 in telemetric communication with the external device 402, such as a programmer, transtelephonic transceiver, or a diagnostic system analyzer. The telemetry circuit 400 is activated by the microcontroller by a control signal 406. The telemetry circuit 400  
5 advantageously allows intracardiac electrograms and status information relating to the operation of the device 310 (as contained in the microcontroller 360 or memory 394) to be sent to the external device 402 through an established communication link 404.

In the preferred embodiment, the stimulation device 310 further  
10 includes a physiologic sensor 408, commonly referred to as a "rate-responsive" sensor because it is typically used to adjust pacing stimulation rate according to the exercise state of the patient. However, the physiological sensor 408 may further be used to detect changes in cardiac output, changes in the physiological condition of the heart, or  
15 diurnal changes in activity (e.g., detecting sleep and wake states). Accordingly, the microcontroller 360 responds by adjusting the various pacing parameters (such as rate, AV Delay, V-V Delay, etc.) at which the atrial and ventricular pulse generators, 370 and 372, generate stimulation pulses.

20 The stimulation device additionally includes a battery 410 that provides operating power to all of the circuits shown in **FIG. 30**. For the stimulation device 310, which employs shocking therapy, the battery 410 must be capable of operating at low current drains for long periods of time, and then be capable of providing high-current pulses (for capacitor  
25 charging) when the patient requires a shock pulse. The battery 410 must also have a predictable discharge characteristic so that elective replacement time can be detected. Accordingly, the device 310 preferably employs lithium/silver vanadium oxide batteries, as is true for most (if not all) current devices.

30 As further shown in **FIG. 30**, the device 310 is shown as having an impedance measuring circuit 412 which is enabled by the microcontroller

360 via a control signal 414. The impedance measuring circuit 412 is not critical to the present invention and is shown for only completeness.

Since stimulation device 310 is intended to operate as an ICD, it must detect the occurrence of an arrhythmia, and automatically apply an appropriate electrical shock therapy to the heart aimed at terminating the detected arrhythmia. To this end, the microcontroller 360 further controls a shocking circuit 416 by way of a control signal 418. The shocking circuit 416 generates shocking pulses under the control of the microcontroller 360 using the techniques described above. The shocking circuit is configured as shown in **FIG. 4** and may be programmed to generate any of the shocking pulse waveforms described above. The shocking pulses are applied to the patient's heart 312 through at least two shocking electrodes, and as shown in this embodiment, selected from the left atrial coil electrode 328, the RV coil electrode 336, and/or the SVC coil electrode 38. As noted above, the housing 340 may act as an active electrode in combination with the RV electrode 336, or as part of a split electrical vector using the SVC coil electrode 338 or the left atrial coil electrode 328 (i.e., using the RV electrode as a common electrode).

Cardioversion shocks are generally considered to be of low to moderate energy level (so as to minimize pain felt by the patient), and/or synchronized with an R-wave and/or pertaining to the treatment of tachycardia. Defibrillation shocks are generally of moderate to high energy level, delivered asynchronously (since R-waves may be too disorganized), and pertaining exclusively to the treatment of fibrillation. Accordingly, the microcontroller 360 is capable of controlling the synchronous or asynchronous delivery of the shocking pulses.

While the invention herein disclosed has been described by means of specific embodiments and applications thereof, numerous modifications and variations could be made thereto by those skilled in the art without departing from the scope of the invention set forth in the claims.